This yields an approximate center-of-mass Schrödinger equation of the usual form:

$$\nabla^2\psi+k^2\psi-(2/\hbar^2)mV\psi=0, \quad \text{(A.4)}$$

where

$$k^2=\frac{1}{\hbar^2}\left[\frac{E^4+(\mu_p{}^2-\mu_\pi{}^2)^2}{4E^2}-\frac{\mu_\pi{}^2+\mu_p{}^2}{2}\right], \quad \text{(A.5)}$$

and

$$mV=\frac{1}{4E^3}[E^4-(\mu_p{}^2-\mu_\pi{}^2]V, \quad \text{(A.6)}$$

are interpreted as the values to be used in Eqs. (1) and (2).

PHYSICAL REVIEW VOLUME 122, NUMBER 3 MAY 1, 1961

Scattering of 2-Bev/c Muons in Carbon and Lead*

G. E. Masek, L. D. Heggie, Y. B. Kim, and R. W. Williams
Department of Physics, University of Washington, Seattle, Washington

(Received November 23, 1960)

The scattering cross section of high-energy μ mesons in carbon and lead has been measured, using a pure, monoenergetic beam of muons obtained with the Bevatron at the Lawrence Radiation Laboratory. Preparation, purification, and measured properties of the beam are described. The median momentum was 2.00±0.03 Bev/c, the spread in momentum was not more than ±3.5%, and the effective contamination due to pions was 4.9×10^{-6}. During the experiment the total number of muons incident on the apparatus was 2.5×10^7. Counter hodoscopes recorded the muons scattered from 14.4 g/cm² of lead and from 27 g/cm² of carbon. Inelastic as well as elastic processes were accepted. Scattered particles were observed at angles up to 12° (momentum transfer ~400 Mev/c). The lead data cover the same range as those cosmic-ray experiments which have appeared to indicate an anomalously large scattering. No anomaly is found; the lead scattering agrees closely with the distribution calculated by Cooper and Rainwater for purely electromagnetic interactions. The carbon data permit a better comparison with theoretical expectations, since one is measuring the single-scattering cross section directly, and one can account for the effects of nuclear structure rather accurately, using electron-scattering data and a detailed theoretical analysis of Drell and Schwartz. The carbon scattering results, based on 300 events in the region 70 Mev/c–400 Mev/c momentum transfer, agree closely with the Drell-Schwartz theory. The upper limits which this result places on a nonelectromagnetic scattering cross section and on a muon form factor are discussed.

I. INTRODUCTION

LOW-ENERGY experiments concerned with muons have indicated that they behave as "heavy electrons."[1,2] However, some experiments on the nuclear scattering of *high-energy* muons[1] have indicated that the experimental cross section at large angles is in excess of that of the electromagnetic prediction. Lloyd and Wolfendale,[3] using cosmic-ray muons of energies between 0.8 Bev and 10 Bev, find that their experimental scattering distributions in Pb tend to follow the Molière *point*-charge multiple-scattering distribution instead of the distribution expected from a realistic consideration of nuclear structure effects. Similarly, McDiarmid,[4] Whittemore and Shutt,[5] further experiments by Lloyd and Wolfendale,[6] and others[1] find the same general behavior for muon energies above 1 Bev, and for scattering angles such that the elastic momentum transfer [$q_0=2k_0\sin(\theta/2)$, where k_0 is the incident momentum and θ the scattering angle in the laboratory system] is between 100 and 200 Mev/c.[7] However, this anomaly is not seen by all such nuclear scattering experiments. The experiments of Watase *et al.*[8] and Amaldi *et al.*[9] (although sensitive to slightly lower incident energies, 0.3 to 1 Bev/c, and slightly lower elastic momentum transfers, 20–100 Mev/c) see no such behavior. Hence, the past experiments on nuclear scattering are not in agreement with each

* This work has been supported by the Office of Naval Research. An account of it will be given in the doctoral thesis of the junior author: L. D. Heggie, thesis, University of Washington, 1961 (unpublished).

[1] For a summary of muon experiments up to 1958, see G. N. Fowler and A. W. Wolfendale, *Progress in Elementary Particle and Cosmic-Ray Physics* (North-Holland Publishing Company, Amsterdam, 1958), Vol. 4, p. 123. Currently, the experiments on the g factor of the muon[2] have shown no differences from the predicted value and hence give further support to the above statement.

[2] R. L. Garwin, D. P. Hutchinson, S. Penman, and G. Shapiro, Phys. Rev. **118**, 271 (1960).

[3] J. L. Lloyd and A. W. Wolfendale, Proc. Phys. Soc. (London) **A68**, 1045 (1955).

[4] I. B. McDiarmid, Phil. Mag. **46**, 177 (1955).

[5] W. L. Whittemore and R. P. Shutt, Phys. Rev. **88**, 1312 (1952).

[6] J. L. Lloyd, E. Rossle, and A. W. Wolfendale, Proc. Phys. Soc. (London) **A70**, 421 (1957).

[7] In addition to the anomalies indicated by these nuclear scattering experiments, the results of R. F. Deery and S. H. Neddermeyer on the high-energy interaction of muons with electrons [Phys. Rev. **121**, 1803 (1961)] indicate a possible deviation from the expected electromagnetic behavior which could be interpreted in terms of a fundamental difference between the muon and electron.

[8] S. Fukui, T. Kitamura, and Y. Watase, Phys. Rev. **113**, 315 (1959).

[9] E. Amaldi and G. Fidecaro, Nuovo cimento **7**, 535 (1950).

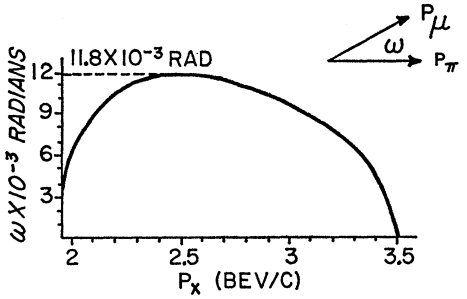

FIG. 1. Relation between the laboratory decay angle ω (defined in the inset) and the laboratory momentum of the resultant muon for the decay in flight of 3.5-Bev/c pions.

other. It should be noted that all of the above experiments on muon nuclear scattering were performed with cosmic-ray muons, and hence were variously plagued by difficulties with momentum determination, muon identification, and, above all else, by low counting rates.

The experiment here described measures the nuclear scattering of muons in carbon and lead up to elastic momentum transfers of 400 Mev/c. The muon beam, produced at the Bevatron, had a well-defined momentum (2.00±0.03 Bev/c), a measured "effective" impurity content of 4.9×10^{-6} (well below that which could contribute to the scattering distribution), and was of sufficient intensity to allow the accumulation of about 2.5×10^7 muons during the entire experiment (compared with 10^4 for most cosmic-ray experiments). The momentum of the particle after the scattering was not measured, and hence the cross sections measured were the total, all final momentum states, into a given angle. The scattering distributions obtained are in good agreement with the electromagnetic predictions and do not agree with those cosmic-ray experiments which have reported an anomalous scattering. We believe this experiment resolves the question of this anomaly: It does not exist.

II. EXPERIMENTAL ARRANGEMENT

Muon Beam

Pion decays in flight were the source of the muons in the experiment. The kinematics for the decay process are shown in Figs. 1 and 2 for a pion energy of 3.5 Bev/c; the following features are pertinent to the muon beam formation: (a) There is a large difference (1.5 Bev/c) between the momentum of parent pions and the momentum of those lowest energy muons which correspond to backward decays in the pion c.m. system; and (b) the muons are confined to very small laboratory angles (±0.68°) with respect to parent pion direction. The large momentum difference permits a relatively clean separation between the pions and the lowest energy muons by magnetic analysis, and the small decay angle insures a relatively large solid angle acceptance for the muon beam. The general arrangement was to first produce an intense momentum-analyzed pion beam (3.5±0.3 Bev/c), allow it to decay along a well-defined drift space, and then momentum analyze again the resulting muon-pion beam, separating the low-energy (2.00 Bev/c) muons from the remaining pions.

TABLE I. Muon- and pion-beam parameters.

Parameter	Value
Muon beam:	
Mean momentum (P_μ)	2.00+0.03 Bev/c
Fractional momentum spread ($\Delta P_\mu/P_\mu$), full width at half maximum	<0.07
Fraction of muons accepted by $\Delta P_\mu/P_\mu=0.07$	0.09
Fraction of muons accepted from total decay solid angle	0.25
Effective area of muon beam at target	6 in.×7½ in.
Maximum muon flux per Bevatron burst (at 2×10^{11} protons per burst)	400
Total muon flux for the experiment	2.5×10^7
Pion beam:	
Mean momentum (P_π)	3.50 Bev/c
Fractional momentum spread ($\Delta P_\pi/P_\pi$), full width at half maximum	0.15
Maximum pion flux per Bevatron burst (at 2×10^{11} protons per burst)	3×10^5
Pion mean decay length (l_π)	218 meters
Decay path length (l), i.e., distance between M_2 and M_3	13.5 meters
Fraction decay in l, (l/l_π)	0.063

The layout for both the muon and parent-pion beam is shown in Fig. 3. Two pion beams were used during the experiment, the 3.5-Bev/c beam, and a 2-Bev/c calibrating beam originating from a second target (T_2) located downstream of the first (T_1). M_1 permitted either of the two beams to be switched onto the quadrupole system Q_1 and Q_2. The focus at F_1 provided a point at which vertical slits could be placed to select the pion momentum spread. During the experiment it was found that the fractional pion content in the final muon beam did not depend upon the pion momentum spread, and hence this slit was left as large as possible, 4 in., to give the largest muon flux. M_2 reanalyzes the pion beam and removes most of the dispersion introduced by the bevatron field. The decay drift space is

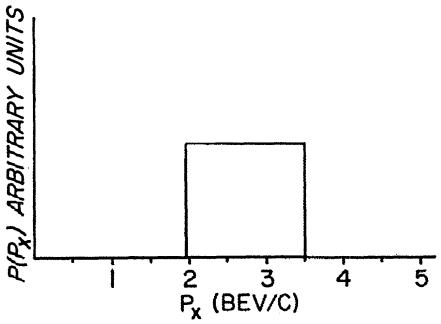

FIG. 2. Distribution of muon laboratory momenta resulting from the decay in flight of 3.5-Bev/c pions.

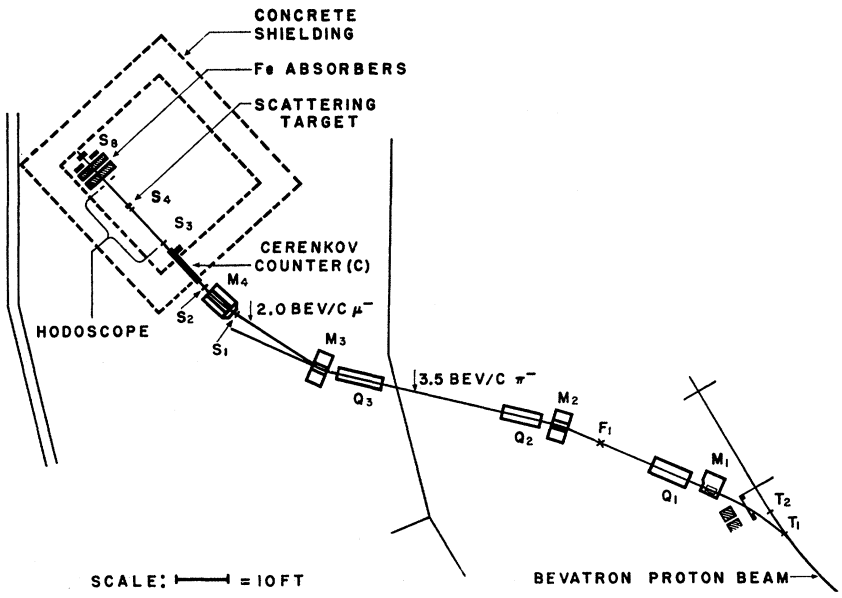

FIG. 3. Experimental arrangement for the pion and muon beams. Also shown are the locations of the hodoscope, and the muon-beam defining counters S_1, S_2, S_3, and S_4. A more detailed drawing of the scattering region is given in Fig. 4.

between M_2 and M_3, where about 6% of the pions decay. M_3 then separates the 2.00-Bev/c muons from the remaining 94% pions. Q_3 provides focusing for the muon beam. Q_3, at optimum setting, increased the muon flux on the target by a factor of 2.5. Finally M_4, aside from providing a second momentum analysis of the muon beam, also reduces the pion contamination which might arise from scatterings at M_3 and provides a means of removing from the beam high-energy electrons (which have been degraded by placing a $\frac{1}{4}$-in. lead sheet in front of M_4). The beam is then directed onto the scattering detectors behind M_4. Table I summarizes the beam parameters discussed here and in Sec. III.

The pion contamination in the muon beam striking the target was measured to be about 3% (see Sec. III). The experiment measures a differential scattering cross section down to about 10^{-28} cm^2/sr whereas the total pion cross section is about 10^{-25} cm^2/sr. Hence, if one requires that the pions contribute less than 10% to the muon yield, a pion contamination less than 10^{-4} is needed. To obtain this degree of purity, we required that the beam pass through a gas threshold Čerenkov counter before the scattering detector and traverse a 42-in. iron absorber after the scattering. These requirements together with the original beam contamination reduced the effective pion contamination to 4.9×10^{-6}. The analysis of beam purity is discussed in Sec. III.

Scattering Detector

The scattering detector was a scintillation counter hodoscope, the geometrical arrangement of which is shown in Fig. 4. The hodoscope was made up of four separate but identical arrays, indicated as A_A, A_B, A_C, and A_D. Arrays A_A and A_B determined the incident direction of a particle onto the target (located immediately behind A_B), while arrays A_B and either A_C or A_D determined the particle's direction after scattering. The arrangement of Fig. 4 permitted a range of scattering angles between 2° and 14°. Each array consisted of 20 individual scintillators which were set vertically (see inset in Fig. 4). Thus a bar does not define a unique space angle, but because of its finite vertical and horizontal extent accepts a small range of space angles. (For angles greater than about 5°, the bars do very nearly define unique space angles.) Each scintillator within an array was viewed by a 931-A photomultiplier. The outputs of these were fed onto a common delay line and then presented by a 4-beam oscilloscope and recorded photographically (Fig. 5).[10] The identification of the scintillator traversed by the event was then made by measuring the delay of the pulse relative to the triggering pulse of the scope. The triggering pulse originated from an auxiliary scintillation counter system which indicated the passage of a particle up the muon channel, and then a scattering into either of the arrays A_C or A_D. Thus the triggering pulse was a coincidence: $SS_{5,6}$, where $S\equiv S_1S_2S_3S_4$ and $S_{5,6}$ means S_5 or S_6. The outputs of the Čerenkov counter, C, the guard counters S_7 and S_9, and S_8 were also displayed on the oscilloscope trace, and the final selection of an "acceptable" scattering event was made visually from the photographic record.

The guard counters S_7 and S_9 helped to eliminate events where a muon was accompanied by a knock-on electron. For example, a knock-on electron made in the target could scatter into the arrays A_C or A_D while the muon provides the appropriate coincidence requirement

[10] In practice the outputs from both ends of the delay line were observed (Fig. 5). This permitted the separation of real events and accidentals which might occur within the total delay time of the line. A more complete description of this hodoscope scheme will be given: G. E. Masek and L. D. Heggie (to be published).

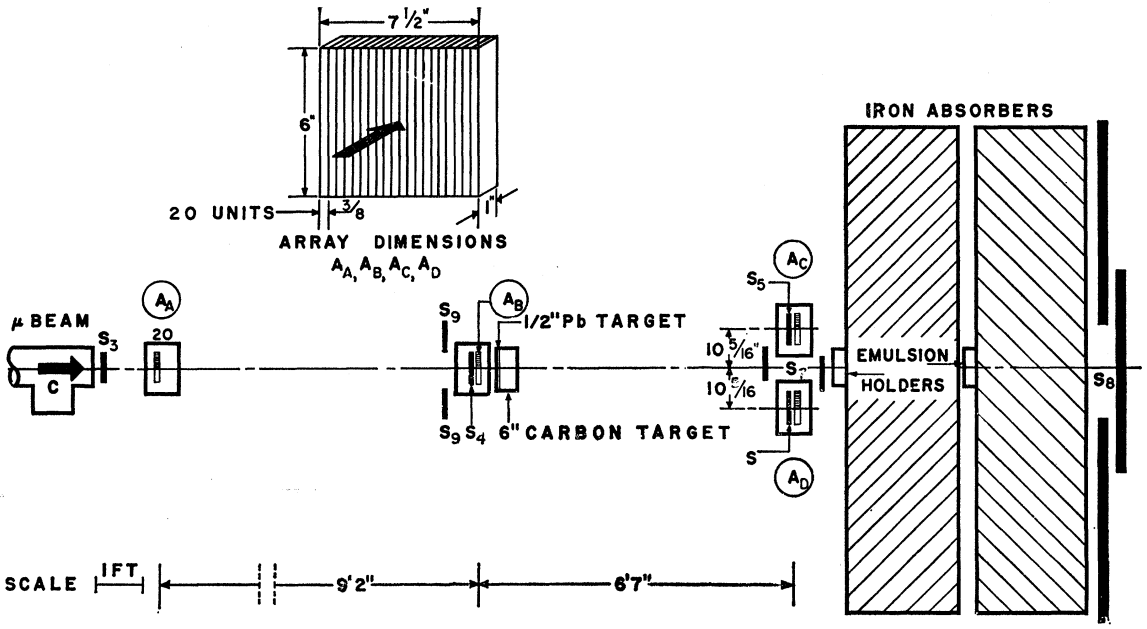

FIG. 4. Experimental arrangement of the scattering detector. The hodoscope arrays are labeled A_A, A_B, A_C, and A_D, and each array consists of 20 scintillators arranged as shown in the inset. The numbers 1 and 20 appearing beside A_A show the sense of the labels i which identify a specific scintillator in A_A. A similar sense holds for j in A_B and k in A_C or A_D. The positions of both the lead and carbon targets are shown, although of course only one or the other was in the beam at one time. The guard counters S_9 actually surround the counter S_4, i.e., top and bottom components of S_9 have been omitted for clarity. The iron absorber is centered vertically on the beam and was 2 feet in height.

in S_8. S_7 would, in general, see the muon, and this type of event could be thrown out. The ratio of knock-on electrons to muon scatterings is largest at large angles. Assuming an efficiency of 99.9% for the anticoincidence counter S_7, we find from an approximate calculation that the differential knock-on background at 9° is about 6%. Similarly, a muon moving outside the channel defined by S but accompanied by a knock-on electron within the channel was detected by S_9. The function of S_8 and C has already been discussed. The final selection of a good event was then a coincidence $SS_{5,6}CS_8\bar{S}_7\bar{S}_9$ and C above a fixed pulse height.

Nuclear emulsion stacks were located at the positions shown in Fig. 4. They were analyzed for stars from pion interactions from which a determination of the pion contamination in the muon beam could be made (see Sec. III). They were also analyzed for muon scatterings; the results of that investigation will be the subject of a subsequent paper.

III. EXPERIMENTAL PROCEDURE AND RESULTS

A. Beam Measurements

Aside from the actual scattering measurements, it was necessary to make determinations of the beam properties, in particular, the momentum of the beam, its structure, and its effective impurity content.

Structure

The structure of the beam was determined in two separate runs in which the oscilloscope was triggered only on S (instead of $SS_{5,6}$ as in the scattering runs) and thus examined the properties of the beam incident on the target. The first run measured the horizontal distribution; the second run, in which the arrays A_A and A_B were rotated 90° about the beam axis, measured the vertical distribution. The results of the horizontal run are shown in Fig. 6, which gives the frequency of particles within an A_A-A_B cell (designated by two numbers ij each of which runs from 1 to 20 and which correspond to scintillator positions as shown in Fig. 4). The distribution in position and incident angle was obtained from these data and the dimensions of the detectors (Fig. 4). In general, the beam was nearly uniform across A_B, had an average angle incident about +0.1° to the center line of A_A and A_B, and had a spread in angles of about ±0.8°. A similar plot of the vertical distribution is uniform on A_B, its average angle coincides with the horizontal, and the spread in angles is about ±0.6°. The correction to the scattering angles due to this vertical distribution is small, being about 6% at the largest. The horizontal distribution is used in the determination of the expected theoretical yield (see Sec. IV).

Momentum

The momentum distribution of the muon beam was measured in a special run in which a ½-in. wide scintillation counter probe S_1' was placed in front of M_4, and the oscilloscope triggered on SS_1' events. This was done for several positions of S_1' across the lateral extent of

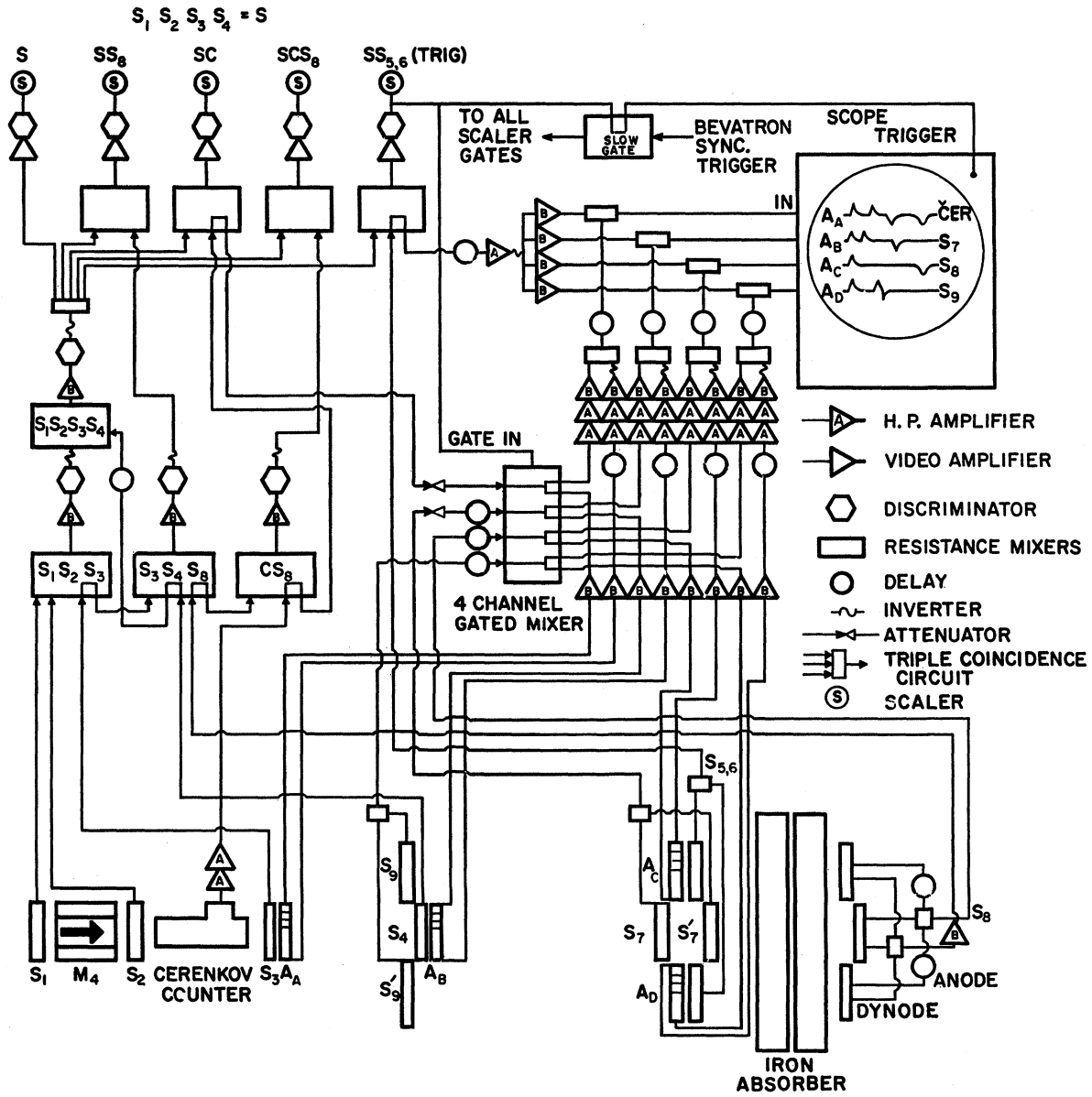

FIG. 5. Block diagram of electronics. The array outputs are displayed on the first half of the oscilloscope traces and are measured relative to the pulse from S_4 which is part of the triggering coincidence. The latter part of the oscilloscope traces contains the information concerning the outputs of S_7, S_8, S_9, and C. These outputs are superimposed at the 4-channel gated mixer.

the muon beam defined by S_1. Distributions in trajectories through A_A and A_B were obtained from the oscilloscope records for each position of S_1'. The three points, determined by the positions of one scintillator from A_A, one from A_B, and S_1', define a radius of curvature through M_4, and hence a distribution in momentum can be obtained from the above trajectory distributions. These measurements give a mean momentum of 2.00 ± 0.03 Bev/c, and an upper limit, fixed by the resolution of the system, to the spread in momentum $\Delta P/P<0.07$. Both of these results agree well with separate determinations from an integral range measurement on the beam.

Impurities

The effective impurity determination involved the separate measurements of the original beam contamination, the transmission efficiency of pions through the Čerenkov counter, and the transmission of pions through the iron absorber. The effective pion impurity is essentially given by the product of these three. These measurements, in turn, required the evaluation of the quantities α_μ, β_μ, and R_μ defined in Table II. During diagnostic runs with the muon beam, scaler information was obtained on the following: N_1, N_2, N_3, and N_4 (see Table IIb); and during runs in which the 2-Bev pion

TABLE II. Efficiency and contamination measurements.

a. Efficiency and contamination measurement summary

Symbol	Definition	Method of measurement	Value[a]
α_π	Transmission efficiency of π's through Čerenkov counter	From shape of Čerenkov pressure curve (Fig. 8)	2.7×10^{-3}
α_μ	Transmission efficiency of μ's through Čerenkov counter	Counter relations in μ beam: $\alpha_\mu\cong N_4/N_3$	0.943
β_π	Transmission efficiency of π's through the Fe absorber	Counter relations in π beam: $\beta_\pi\cong(N_3'/N_1')(1+R_\mu)-R_\mu\beta_\mu$	0.052
β_μ	Transmission efficiency of μ's through the Fe absorber	Counter relations in μ beam: $\beta_\mu\cong N_4/N_2$	0.984
R_μ	Ratio of μ's to π's in the π beam (N_μ'/N_π')	Counter relations in π beam: $R_\mu\cong(N_2'/N_1')(\alpha_\mu-N_2'/N_1')^{-1}$	0.065
R_π	Ratio of π's to μ's in the μ beam (N_π/N_μ)	a. Emulsion stars	0.025 ± 0.005
		b. Čerenkov pressure curve extrapolations (Fig. 8)	0.032 ± 0.002
		c. Counter relations in μ beam: $R_\pi\cong(N_1/N_2)\alpha_\mu-1$	0.038 ± 0.004
		d. Average of (a), (b), and (c)	0.032 ± 0.002
R	Effective pion contamination in muon beam	$R=R_\pi(\alpha_\pi/\alpha_\mu)(\beta_\pi/\beta_\mu)$	4.9×10^{-6}

b. Counter relations to above parameters

Coincidence condition (see Fig. 5)	Yield symbol	Measures[b, c, d]	Total counts during diagnostic runs: μ beam	π beam
S	N_1	$N_1=N_\mu(1+R_\pi)$	6.09×10^5	1.3×10^5
SC	N_2	$N_2=N_\mu(\alpha_\mu+R_\pi\alpha_\pi)$	5.50×10^5	7.43×10^3
SS_8	N_3	$N_3=N_\mu(\beta_\mu+R_\pi\beta_\pi)$	5.76×10^5	1.39×10^4
SCS_8	N_4	$N_4=N_\mu(\alpha_\mu\beta_\mu+R_\pi\alpha_\pi\beta_\pi)$	5.42×10^5	7.1×10^3

[a] Errors are given on the separate determinations of R_π to show the consistency of the different methods of measurement. Errors on other quantities are omitted since they only reflect as small errors in R, and even large errors in R do not affect the muon yield because the value of R is so small (see Table IV).

[b] The quantities N_μ and N_π are the number of muons and pions, respectively, in the μ beam.

[c] The same relations hold for the π beam except the subscripts π and μ are reversed and we use the primed symbols to designate π-beam quantities, i.e., N_1', $N_2'\cdots$, etc.

[d] A small electron contamination due mostly to "knock-on's" (see Sec. II) is not included in these relations. If this is included, the expression for R_π becomes $R_\pi=\alpha_\mu-(N_2/N_1)-R_e(1-\alpha_e)$, where the e subscripts pertain to the electron contamination. Comparisons of this relation with the other methods of determining R_π (see above) show that the upper limit on R_e is 0.015. This does not contribute an appreciable error to the above expressions.

beam was brought down the muon channel the quantities N_1', N_2', N_3', and N_4' were measured. These, together with the information obtained from the Čerenkov pressure runs (see below), are combined in the manner indicated in Table II to give the results shown there.

HORIZONTAL DISTRIBUTION OF MUON FLUX

	1	2	3	4	5	6	7	8	9	10	11	12	13	14	15	16	17	18	19	20
1	7	15	21	26	25	20	14	13	2		1					1		1		
2	3	9	14	17	17	21	14	11	9	1	3						1			
3	1	8	18	18	19	25	25	20	12	3	2	1			2					
4		3	6	13	21	20	16	14	10	8	6									
5			3	10	22	13	23	18	20	22	7	2								
6			1	9	10	12	19	11	19	18	14	2	1							
7				3	6	13	19	11	22	18	16	8	3	2	1					
8					6	16	24	30	27	15	18	9	7	2		1	1			
9					2	8	20	25	28	29	32	15	14	7	2	1	1			1
10						1	15	15	18	27	28	24	23	10	9					
11					1	1	7	14	18	25	42	34	33	34	12	1		1		
12							2	16	14	25	32	32	35	32	11	13	1			
13								4	10	22	34	24	43	33	25	20	7			
14									4	7	25	26	34	36	30	26	9	2	1	1
15									2	3	14	19	24	33	34	35	17	13	1	
16				1			1		1	4	7	6	15	24	23	26	19	9	2	
17										2	6	13	13	17	21	25	23	9	6	1
18										1		5	5	10	19	22	23	26	6	2
19			1			1							13	17	16	20	17	29	25	7
20									1				3	13	12	22	20	15	20	13

i ⟶ (rows)

j ↓ (columns)

FIG. 6. Horizontal distribution of the incident beam. The labels 1–20 along the horizontal and vertical are the numbers of each scintillator in arrays A_A and A_B, respectively, as shown on Fig. 4. The value appearing in each box ij is the number of particles that passed through scintillator i of A_A and j of A_B for a total incident flux of 3137 particles. These values are designated as n_{ij} in the text.

The transmission efficiency of the Čerenkov counter for particles of the muon beam was measured as a function of the pressure within the Čerenkov counter.[11] The results are shown in Figs. 7 and 8 in which the efficiency rises sharply at the muon threshold, levels off near 96%, then rises again to almost 100% near the pion threshold. These pressure curves, together with the extrapolations shown in Figs. 7 and 8, can be used to evaluate the quantities R_π and α_π of Table II. The values so obtained are entered in Table II.

The value of the effective pion contamination (R), obtained by combining α_π/α_μ, β_π/β_μ, and R_π, is 4.9×10^{-6}. α_π is, of course, a function of the momentum distribution of the pions within the muon beam. In treating α_π as an independent contamination factor, we must assume that the pion and muon momentum distributions within the muon beam are the same (or that the pions are of lower momentum, in which case α_π is effectively smaller). This assumption is given support by the shape of the Čerenkov pressure curve which shows the definite hump due to pions of about 2 Bev/c and which can account for all the pions meas-

[11] The gas Čerenkov counter used in the experiment is similar in design to those described by J. H. Atkinson and V. Perez-Mendez, Rev. Sci. Instr. **30**, 864 (1959). It is 10 ft long, 13 in. in diameter, and filled with CO_2. The Čerenkov light is reflected by a front-surface mirror inclined at 45°, and focused onto a 7264 photomultiplier by a 13-in. diameter Fresnel lens (focal length 12 in.). The instrument is to be described in greater detail in another journal.

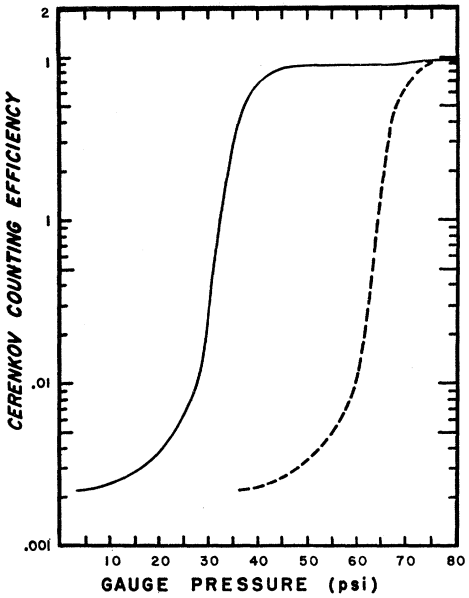

FIG. 7. Čerenkov counter transmission efficiency in the muon beam as a function of the pressure within the counter. For momenta of 2 Bev/c, the muon and pion thresholds are 49.4 psi and 87.6 psi, respectively. The dashed curve is an extrapolation of the shape of the curve (which is predominantly due to muons) to the pion threshold, and thus represents the expected shape for a pure pion beam.

ured by other means (see Table II). Further, the double magnetic analysis of the muon beam by M_3 and M_4 makes it extremely difficult for *higher* energy pions to get into the system.

B. Scattering Runs

Two targets were used in the experiment, 27 g/cm^2 of carbon and 14.4 g/cm^2 of lead. "Target in" runs were alternated with "target out" runs; the total incident flux was recorded on the scalers, 1.6×10^7 for the carbon, 3.4×10^6 for the lead, and 4.9×10^6 for target out. The film was scanned for acceptable events (see Sec. II) and their nominal scattering angles φ were measured from the array traces. The nominal scattering angle, which is identified with a combination of scintillators i, j, k, is the scattering angle of a particle confined to the horizontal plane which passes through the center of scintillator i in A_A, is scattered in the center of j in A_B, and finally passes through the center of scintillator k in A_C or A_D. The weighted average of the space scattering angles over the three-scintillator combination is, of course, very nearly equal to this nominal scattering angle for large ($>5°$) angles (again assuming the scattering occurs in A_B instead of the target). These data are presented as histograms in Figs. 9, 10, 11 for lead, carbon, and target out, respectively. In Figs. 12 and 13 the experimental yield for lead and carbon is shown as an integral plot in which the target-out subtraction has been made. The errors shown are statistical only.

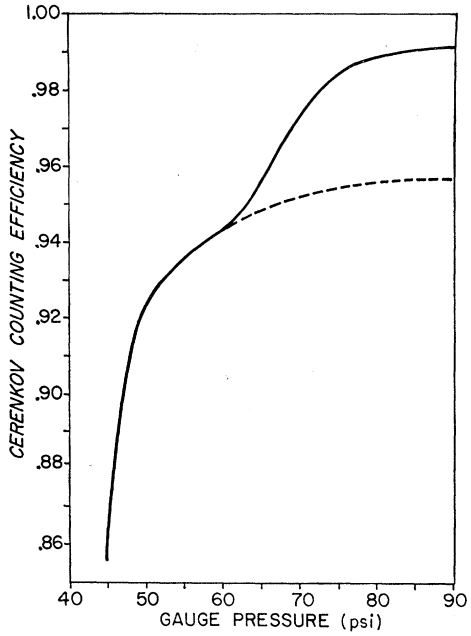

FIG. 8. Čerenkov counter transmission efficiency in the muon beam as a function of the pressure within the counter. Same as Fig. 7, except that the top of the curve is shown in detail and the breaks in the curves due to muons and pions at their respective threshold pressures are much more noticeable. The extrapolation here shown is what would be expected for the shape of the muons alone, and hence the pion contamination can be obtained from the difference.

IV. THEORETICAL YIELD

To relate the observed yield of scattered particles to the cross section we must take into account both the acceptance function of the hodoscope and the spatial and angular distribution of the incident muon beam. The most convenient comparison of theory and experiment can be made by calculating the expected distri-

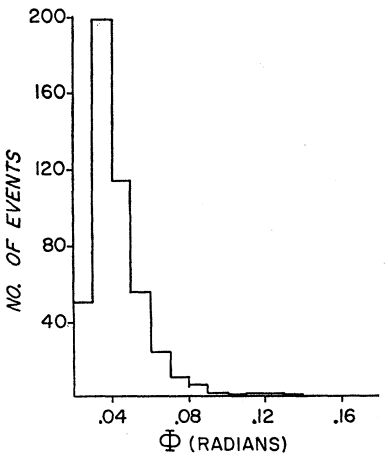

FIG. 9. Histogram showing the angular distribution of 2-Bev/c muons obtained when the 14.4-g/cm^2 lead target was placed in the position shown in Fig. 4. The nominal scattering angle φ is defined in the text. Total incident muon flux was 3.38×10^6.

TABLE III. Numerical evaluation of the Drell-Schwartz cross section for the scattering, elastic plus inelastic, of 2.00-Bev/c muons by carbon.

Scattering angle θ	2.29°	3.44°	4.59°	5.73°	8.03°
Elastic momentum transfer, q_0 (Mev/c)	80	120	160	200	280
Proton form factor, $f^2(q_0)$	0.973	0.941	0.897	0.845	0.719
Two-body form factor, f_2	0.70	0.44	0.22	0.070	−0.015
$Z+Z(Z-1)f_2$	27.0	19.2	12.6	8.10	5.55
Magnetic scattering[a]	0.06	0.17	0.40	0.74	1.57
Cross section, $\partial\sigma/\partial\Omega$ (mb/sr)	209	28.9	5.88	1.53	0.272
Multiple-scattering correction[b]	25%	13%	9%	5%	2%
Scattering distribution in 27 g/cm², $P(\theta)$ (sr^{-1})	0.356	0.0444	0.00868	0.00223	0.00038
Change in $P(\theta)$ caused by including Fowler-Watson correlations[c]	−1.6%	−3.2%	−6.0%	−10%	−14%
Change in $P(\theta)$ caused by a 6% change in shell-model parameter, ν[d]	1.6%	3.4%	5.4%	4.1%	0.7%

[a] The final term in Eq. (2), spin correlation, has been treated in an approximate way, but the term is small so that an error here would have a very small effect on $P(\theta)$.
[b] From L. Cooper and J. Rainwater, reference 12, p. 500.
[c] See Fowler and Watson, reference 20. This estimate uses their form for "Cc" in their Eq. (3.26).
[d] 6% is suggested as a limit of error on the value of ν as determined from electron scattering.

bution in angle (actually nominal angle as explained above), and casting the experimental results in the same form. The expected theoretical yield for the hodoscope in both the carbon and lead runs was calculated from the following expression:

$$\frac{\Delta Y}{\Delta\theta'}(\theta')=\epsilon(\theta',\varphi)P(\theta)\Big|_{\theta=\varphi}\sum_{i,j,k}^{\varphi}\nu_{ij}\Delta\Omega_{jk}, \qquad (1)$$

where i, j, k are each numbers designating a specific scintillator within the arrays A_A, A_B, A_C, and A_D, respectively; i and j are numbers from 1 to 20, and k is a number from 1 to 40. ν_{ij} is the number of muons incident on the bar combination ij during the entire run; it is computed from the total incident flux for the run N_i and the data of Fig. 9, i.e., $\nu_{ij}=N_i n_{ij}/\sum_{ij} n_{ij}$, where n_{ij} is the number in each cell of Fig. 9. $\Delta\Omega_{jk}$ is the solid angle subtended by the bar k in A_C or A_D from the bar j in A_B; it is very nearly a constant for all jk contaminations. φ is the nominal scattering angle (see Sec. III). θ' is the nominal scattering angle, but corrected for the target position. $\Delta\theta'$ is the nominal angular spread associated with a single bar at θ'. $P(\theta)|_{\theta=\varphi}$ is the total scattering probability per steradian for the process evaluated at φ. $\epsilon(\varphi,\theta')$ is a correction factor which includes a correction for the target position not being coincident with A_B, and a correction due to the difference between the nominal angle and the weighted average space angle over the finite bar dimensions. The sums are carried out over all i, j, k combinations with nominal angles φ within the range $\varphi\pm\frac{1}{2}\Delta\varphi$.

Evaluation of the Cross Sections

Lead

In lead the scattering distribution is dominated by multiple scattering at all but the largest angles. The distribution $P(\theta)$ used in expression (1) was obtained from the multiple-scattering distribution of Rainwater

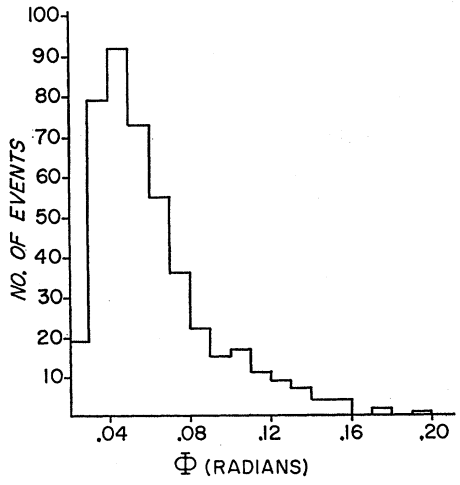

FIG. 10. Histogram showing the angular distribution of 2-Bev/c muons obtained when the 27.0-g/cm² carbon target was placed in the position shown in Fig. 4. The nominal scattering angle φ is defined in the text. Total incident muon flux was 16.4×10^6.

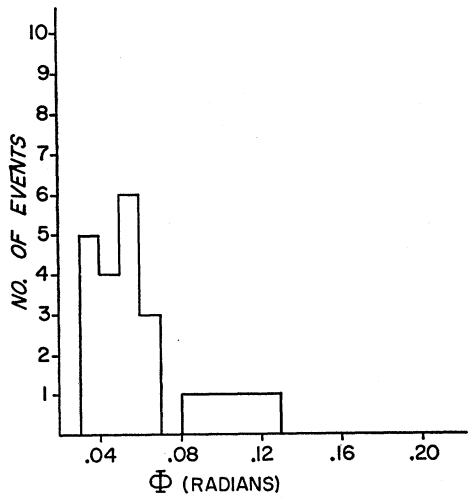

FIG. 11. Histogram showing the angular distribution of 2-Bev/c muons obtained when no target was placed in the beam, i.e., during the "target out" runs. The nominal angle φ is defined in the text. Total incident muon flux was 4.88×10^6.

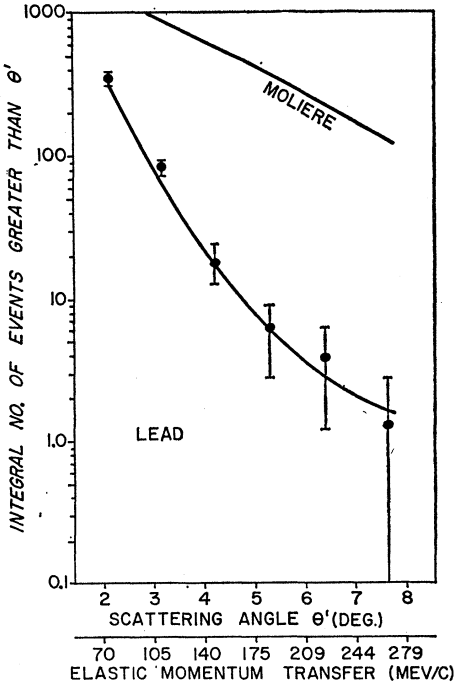

FIG. 12. Curves showing the theoretical and experimental *integral* angular distribution of 2-Bev/c muons scattered in 14.4 g/cm² of lead. Target-out subtractions have been made to the experimental points. The errors shown are statistical only. The theoretical distribution was obtained by integrating expression (1) of the text, with appropriate substitutions for lead, over all angles *greater* than θ'. The nominal scattering angle θ' is defined in the text and is very nearly equal to the true space scattering angle for angles larger than about 5°. The second abscissa is the elastic momentum transfer associated with the angle θ'. Also shown is the expected theoretical yield for the Molière distribution which assumes a point charge for the nucleus.

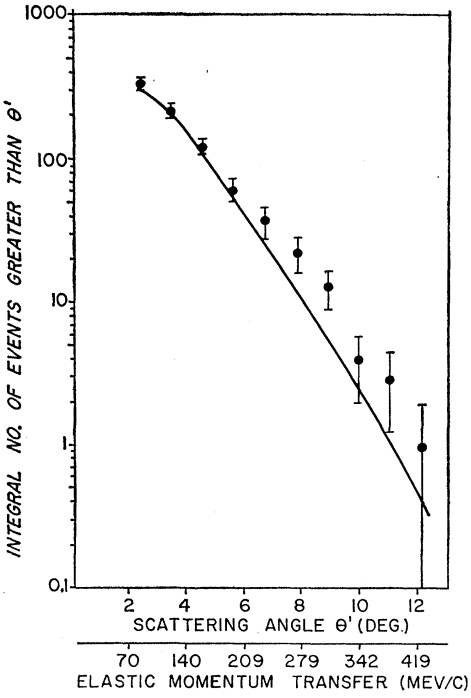

FIG. 13. Curves showing the theoretical and experimental *integral* angular distributions of 2-Bev/c muons scattered in 27.0 g/cm² of carbon. Target-out subtractions have been made to the experimental points. The errors shown are statistical only. The theoretical curve was obtained by integrating expression (1), with the appropriate substitutions for carbon, over all angles greater than θ'. The nominal scattering angle θ' is defined in the text and is very nearly equal to the true space scattering angle for angles *greater* than about 5°. The second abscissa is the elastic momentum transfer associated with the angle θ'.

and Cooper.[12] We have used directly their nuclear form factor expression, the elastic part of which checks quite well with the results of Hofstadter *et al.*[13] for Bi. Independent calculations using both methods of reference 12 were made and found to agree within 10%. The results of these calculations, converted to space angle distributions by inverting the approximate method described in reference 12, were used in Eq. (1). The result appears as the solid curve in Fig. 12.

Carbon

In carbon, the multiple scattering is only a small correction throughout the region of greatest interest (see Table III). The experiment therefore provides a direct measurement of the single scattering cross section. The work of Drell and Schwartz[14] has been used to evaluate this cross section. They have applied conventional electromagnetic theory, including the effects of nuclear structure, recoil, magnetic scattering, and nucleon form factors, to precisely the problem at hand: the "low resolution" (all final energies accepted)[15] differential cross section for scattering of a muon or electron from a light nucleus. They give:

$$\frac{\partial\sigma}{\partial\Omega}=\sigma_0 f^2(q_0)\Big\{Z+Z(Z-1)f_2+\frac{Zq_0^2}{2AM^2}$$
$$+[2\sec^2(\theta/2)-1]\Big[\frac{2}{3}\frac{Z}{AM}\langle T\rangle+\frac{q_0^2}{4M^2}(Z\mu_p^2+N\mu_n^2$$
$$+\tfrac{1}{3}\sum_{i\neq j}\sum\langle\boldsymbol{\sigma}_i\cdot\boldsymbol{\sigma}_j\mathbf{y}_i\cdot\mathbf{y}_j e^{i\mathbf{q}_0\cdot\mathbf{r}_{ij}}\rangle)\Big]\Big\}. \quad (2)$$

The notation is that of Drell and Schwartz.[14] σ_0 is related to the Mott cross section; $f(q_0)$ is the proton form factor; $\mathbf{q}_0$ is the momentum transfer to the carbon nucleus in an elastic scattering through angle θ; the final three terms are magnetic scattering. Nuclear structure enters almost entirely through the form

[12] L. N. Cooper and J. Rainwater, Phys. Rev. **97**, 492 (1955).
[13] B. Hahn, D. G. Ravenhall, and R. Hofstadter, Phys. Rev. **101**, 1131 (1956).
[14] S. D. Drell and C. L. Schwartz, Phys. Rev. **112**, 568 (1958).

[15] Actually, the iron absorber limits the scattered muons to momenta greater than 1.36 Bev/c. However, the contribution to the total cross section for scatterings with momentum losses greater than 0.64 Bev/c is extremely small.

factor for two-body correlations,

$$f_2=\int \varphi_0^*\varphi_0 e^{iq_0\cdot(r_1-r_2)}d\tau_1\cdots d\tau_Z. \quad (3)$$

Expression (2) has been experimentally checked by Friedman[16] who finds excellent agreement for the scattering of electrons by deuterium. If the nuclear ground-state wave function φ_0 were known precisely, expression (2) should be accurate, in the range of this experiment, to better than 5%, according to Drell and Schwartz.

The evaluation of the various terms of (2) is summarized in Table III. The quantity f_2 was evaluated using the results of Gatto[17] who has calculated f_2 for C^{12} using oscillator shell-model wave functions in j-j coupling:

$$f_2=e^{-x}\left(1-\frac{8}{15}x+\frac{4}{135}x^2\right), \quad (4)$$

where $x=q_0^2/2\nu$, and ν is the size parameter of the oscillator wave function. The value of ν has been taken to be 3.64×10^{25} cm^{-2} in agreement with the elastic electron scattering data of Hofstadter.[18]

The shell-model calculation does not include any correlations caused by nucleon-nucleon forces.[19] A very rough estimate of the effect of short-range correlations, based on the work of Fowler and Watson,[20] is included in Table III and shows that the neglect of these correlations could be the largest uncertainty in the theoretical evaluation of the yield, i.e., the uncertainty could be as high as 15% at the highest momentum transfers considered. Drell and Schwartz estimate a much smaller effect. Also not included is an estimated contribution to the scattering cross section at high momentum transfers of about 3% connected with pion production and related effects. The results of this cross-section evaluation are used in expression (1). The solid curve of Fig. 13 is the integral of expression (1) over all angles greater than θ'.

Table IV gives a summary of systematic errors and corrections for this experiment.

TABLE IV. Summary of systematic errors and corrections which have not been included in the theoretical yield curves of Figs. 12 and 13. The corrections apply to the theoretical yields, the positive sign being associated with an increase in the yield. The symbols (C) and (Pb) indicate that the error or correction applies to carbon or lead, respectively. Where values are not shown, they are negligible.

Description of errors and corrections	Value 3°	Value 7°
Uncertainty in theoretical yield due to:		
Central momentum uncertainty (C)	±0.04	±0.05
Central momentum uncertainty (Pb)	±0.09	±0.05
$\epsilon(\theta',\varphi)$ uncertainty (C)	±0.04	±0.025
$\epsilon(\theta',\varphi)$ uncertainty (Pb)	±0.065	±0.02
Uncertainty associated with nucleon-nucleon correlation (C)	±0.02	±0.15
Uncertainty associated with Drell-Schwartz sum rule (C)		±0.05
Uncertainty in Rainwater-Cooper multiple scattering distribution (Pb)	±0.02	±0.10
Corrections for:		
Muon momentum spread (C)	+0.01	+0.01
Muon momentum spread (Pb)	+0.015	+0.01
Knock-on electrons (C and Pb)	+0.006	+0.048
Pion contamination in muon beam (C and Pb)	<0.001	+0.015
Incident beam vertical distribution (C and Pb)	+0.06	<0.001
Pion production in the cross section (C)		+0.03

V. DISCUSSION

Lead

The lead nucleus was selected as a target material to allow a direct comparison between our results and those of the cosmic-ray experiments that have reported the anomalous scattering. Most of these observers[1,3–6] have used lead as the scattering material. Lloyd and Wolfendale[3] and McDiarmid[4] have also used iron, and from the comparison between their iron and lead results it was concluded that the anomalous scattering was *not* proportional to Z (or A) as might be expected for some short-range muon-nucleon interaction. Instead, the effect is more pronounced in lead and consistent with a higher power Z dependence (e.g., Z^2). In addition to the experimental results and the Rainwater-Cooper predictions, Fig. 12 also shows the theoretical yield expected if the lead nucleus is considered as a point charge (Molière distribution). It will be recalled (Sec. I) that the anomalous scattering distribution is reported to follow closely this Molière distribution. Our results are in the same energy and angular range as those reported to give anomalous scattering. It is seen from Fig. 12 that the differences between our data and the Molière distribution are quite large, being about 90 standard deviations throughout most of the range of the experiment. Thus our results are in direct contradiction with those experiments reporting this anomalous cross section. Our results are found to agree quite closely with the predictions of Rainwater and Cooper.

Carbon

The lead results show that no *large* anomaly exists in the nuclear scattering of muons. More subtle effects may, however, still exist, and for this reason most of the running time was devoted to the scattering in carbon where it might be expected that deviations from the accepted electromagnetic theory would be more easily observed. Such deviations might occur either as

[16] J. I. Friedman, Phys. Rev. **116**, 1257 (1959).
[17] R. Gatto, Nuovo cimento **10**, 1559 (1953).
[18] H. F. Ehrenberg, R. Hofstadter, U. Meyer-Berkhout, D. G. Ravenhall, and S. E. Sobottka, Phys. Rev. **113**, 666 (1959).
[19] The correlations due to the Pauli principle have, of course, been included because the wave function is antisymmetrized.
[20] T. K. Fowler and K. M. Watson, Nuclear Phys. **13**, 549 (1959).

TABLE V. Pion scattering results in carbon. The expected numbers for the muon scattering runs are calculated using the measured numbers, the incident fluxes, and the measured π contamination in the μ beam, R.

Angle θ' (deg)	No. of π^- scattered through angles greater than θ': Measured No. for 5.8×10^4 incident π^-	No. of π^- scattered through angles greater than θ': No. expected during μ-scattering run on carbon with $N_\mu=1.64\times10^7$ and $R=4.9\times10^{-6}$
2	435	0.411
3	418	0.395
4	365	0.345
5	300	0.284
6	231	0.219
7	187	0.176
8	144	0.135
9	111	0.105
10	63	0.061
11	34	0.032
12	10	0.009
13	7	0.006
14	1	0.001

a short-range muon-nucleon interaction or as a breakdown in the accepted quantum electrodynamics interaction for the muon, which would manifest itself as a muon-nucleon form factor different from that of the electron-nucleon form factor. Such effects would be more easily observed in a low-Z material where the multiple scattering is not dominant and the theoretical predictions are on a much firmer basis. It should further be noted that both effects would be more pronounced at higher q.

Our experimental results on carbon are shown in Fig. 13 together with the predictions of Drell and Schwartz. It is seen that within the experimental and theoretical accuracy, they are in agreement. If one interprets the results of Lloyd and Wolfendale in terms of a per nucleon anomalous cross section, approximately 2000 events would have been predicted for scatterings greater than 3° as compared to the 250 events we obtained. Even if, as suggested by the comparison of their iron or lead data, the anomalous cross section is proportional to Z^2, about 200 events at angles greater than 5° should have been seen. Clearly both such possibilities are far outside the limits permitted by our experiment, and so again we are in direct contradiction with the experiments which have seen such an anomaly.

If we now make the assumption that the angular distribution of the anomalous cross section, if it exists, is similar to the distribution obtained from the nuclear scattering of pions, we can set an upper limit to the anomalous cross section. We measured directly in the hodoscope the angular distribution of 2-Bev/c pions scattered in the carbon target. The results appear in Table V. The comparison of the pion angular distribution with that of the muons, Fig. 13, gives an upper limit to such an anomalous cross section of

$$\left.\frac{d\sigma}{d\Omega}\right|_{\text{anom}} < 1.5\times10^{-29} \text{ cm}^2/\text{sr-nucleon}.$$

We now examine the extent to which this experiment tests the limits of quantum electrodynamics for the muon at small distances. We introduce a form factor $F(q,\Lambda)$ which multiplies the cross section of expression (2) and which approximates the modifications to (2) expected from a breakdown in quantum electrodynamics at some characteristic distance $1/\Lambda$. Note that expression (2) already contains the form factor f which has been experimentally measured in electron-proton scattering and which is usually attributed to a nucleon structure (but it can also be interpreted as a breakdown in quantum electrodynamics). Hence $F(q,\Lambda)$ is an additional form factor which we associate with the muon. Following Drell,[21] the form of $F(q,\Lambda)$, which holds for $(q\hbar/\Lambda)^2\ll1$, is chosen to be

$$F(q,\Lambda)=[1+2(q\hbar/\Lambda)^2]^{-1}. \quad (5)$$

Using various values for Λ, we have obtained modified expressions for (2) and have examined to what extent these modified expressions were compatible with our experimental results. We have done this (a) using only the statistical errors, and (b) assuming an additional 20% systematic error on all points with q's greater than 1 f^{-1}. The limits on $1/\Lambda$ from this procedure at the 95% confidence level are:

(a) $1/\Lambda<0.43$ f using statistical errors only;
(b) $1/\Lambda<0.58$ f using statistical errors and a 20% systematic error.

These limits are more stringent than those which can be set from the recent experiments on the anomalous magnetic moment of the muon by Garwin *et al.*[2] They obtain for the g value of the muon (using the muon mass measurements of Lathrop *et al.*[22])

$$g_\mu=2(1.00113_{-0.00012}{}^{+0.00016}),$$

or

$$g_\mu=2[1+(\alpha/2\pi)(1_{-0.13}{}^{+0.11})].$$

The fractional correction to $\alpha/2\pi$ caused by a breakdown at the muon vertex or in the photon propagator is[23] $\frac{2}{3}(\hbar\Lambda/m_\mu c)^{-2}$ where m_μ is the muon rest mass. This gives at the 95% confidence level $1/\Lambda<1.03$ f.[24] It should be noted, however, that neither measurement, the muon scattering experiment here described or the

[21] S. D. Drell, Ann. Phys. **4**, 75 (1958).
[22] J. Lathrop, R. A. Lundy, S. Penman, V. L. Telegdi, R. Winston, D. D. Yovanovitch, and A. J. Bearden, Nuovo cimento **17**, 114 (1960).
[23] V. Berestetskiĭ, O. Krokhin, and A. Khlebvilov, J. Exptl. Theoret. Phys. (U.S.S.R.) **30**, 788 (1956) [translation: Soviet Phys.—JETP **3**, 761 (1956)].
[24] *Note added in proof.* See however the new work of G. Charpak, F. J. M. Farley, R. L. Garwin, T. Muller, J. C. Sens, V. L. Telegdi, and A. Zichichi, Phys. Rev. Letters **6**, 128 (1961).

measurement of the muon magnetic moment, test general quantum electrodynamics to as small a distance as e-p scattering or the Lamb shift.

The electron-proton scattering results give a limit on the combined effects of a finite proton size and a modified photon propagator (assuming there is no breakdown at the electron vertex). The proton form factor f has already included these effects in expression (2). Hence, the above limits on $1/\Lambda$ set by the muon scattering experiment described here will apply only to the muon vertex and can be interpreted as a limit on the muon size. Using the larger of the two values above, this gives

$$(r_{\text{muon}}^2)^{\frac{1}{2}}=6^{\frac{1}{2}}/\Lambda<1.4 \text{ f}.$$

To summarize the results of this experiment, we find no evidence for an anomaly in the scattering of high-energy muons from either lead or carbon. Our results are in contradiction to those experiments which have reported such anomalies. We do find good agreement with the expected electromagnetic predictions.

ACKNOWLEDGMENTS

The authors would like to express their thanks to W. A. Wenzel and B. Cork for their suggestions and help. We are indebted to S. H. Neddermeyer, S. Kaneko, D. Bodansky, H. B. Silsbee, and J. J. Lord for discussions and suggestions. We wish to thank E. M. Henley for his generous aid with the theoretical interpretations of the experiment. We would like to express our appreciation to W. H. Barkas and N. Nichols for their aid during the runs. C. Y. Kim, E. Platner, S. B. Curtis, R. J. Swanson, and R. F. Deery gave valuable assistance during the conduct of the experiment. We also wish to thank E. Lofgren and all members of the Bevatron staff and crew for their invaluable assistance.

PHYSICAL REVIEW VOLUME 122, NUMBER 3 MAY 1, 1961

π^+-p Elastic Scattering at 310 Mev: Recoil-Nucleon Polarization*

JAMES H. FOOTE,† OWEN CHAMBERLAIN, ERNEST H. ROGERS, HERBERT M. STEINER, CLYDE E. WIEGAND, AND THOMAS YPSILANTIS
Lawrence Radiation Laboratory, University of California, Berkeley, California

(Received December 27, 1960)

The recoil-proton polarization in π^+-p elastic scattering at 310-Mev incident-pion laboratory kinetic energy has been experimentally measured at four scattering angles with scintillation counters. Polarization values obtained, related rms experimental errors, and mean center-of-mass recoil angles are: $+0.044\pm0.062$ at 114.2 deg, -0.164 ± 0.057 at 124.5 deg, -0.155 ± 0.044 at 133.8 deg, and -0.162 ± 0.037 at 145.2 deg. The sign of the polarization is defined to be positive when a preponderance of the recoil protons had their spin vectors pointing in the direction of $\mathbf{p}_i\times\mathbf{p}_f$, where this quantity is the cross product of the initial and final momentum vectors of the conjugate pions. A beam of 1×10^6 pions per sec incident upon a 1.0-g/cm^2-thick liquid-hydrogen target produced the recoil protons, which were then scattered by a carbon target at a mean energy varying with recoil angle from 113 to 141 Mev. The polarization of the recoil protons was analyzed by measuring the asymmetry produced in the carbon scattering. A proton beam of known polarization was used to determine the analyzing ability (measured asymmetry divided by the polarization of the incident protons) of the system at each recoil angle. Values obtained for the analyzing ability range from 0.41 to 0.57.

I. INTRODUCTION

TO investigate π^+-p and π^--p elastic scattering, which are processes of fundamental importance to the understanding of nuclear phenomena, we can measure the differential cross section, the total cross section, and the polarization of the recoil protons as a function of scattering angle.[1] Although pion-proton cross sections have been measured by many experimenters at many energies, the accuracy and completeness of the experimental data can be considerably improved upon. In contrast to the numerous cross-section results, few measurements exist of the recoil-proton polarization in elastic pion-proton scattering. This scarcity of data is due to the difficulty of obtaining pion beams of high energy and, in addition, high intensity. Beams with both of these characteristics are needed so that the polarization of the recoil protons can be satisfactorily analyzed. If the flux of these protons were not adequate or if their energy were too low, we would not be able to determine their polarization with the desired accuracy.

In former analyses of pion-proton scattering data in

* This work was done under the auspices of the U. S. Atomic Energy Commission.

† Now at Lawrence Radiation Laboratory, Livermore, California.

[1] Fermi first showed, theoretically, that one can in general expect the recoiling protons to be polarized, this polarization being perpendicular to the plane of the scattering. See E. Fermi, Phys. Rev. **91**, 947 (1953).